HHS Public Access

Author manuscript

Health Phys. Author manuscript; available in PMC 2020 May 01.

Published in final edited form as:

Health Phys. 2019 May ; 116(5): 590–598. doi:10.1097/HP.0000000000000971.

A dosimetry study of portable x-ray fluorescence *in vivo* metal measurements

Aaron J. Specht[1,*], **Xinxin Zhang**[2], **Benjamin D. Goodman**[3], **Ed Maher**[1], **Marc G. Weisskopf**[1], and **Linda H. Nie**[2]

[1]Harvard T.H. Chan School of Public Health Boston, MA

[2]School of Health Sciences, Purdue University West Lafayette, IN

[3]Saint Francis Medical Center, Cape Girardeau, MO

Abstract

Portable x-ray fluorescence (XRF) devices have grown in popularity for possible metal exposure assessment using *in vivo* measurements of bone and toenail. These measurements are accompanied by a small radiation dose, which is typically assessed by radiation safety committees to be minimal. However, an understanding of precise dose under different instrument conditions is still needed. This study set out to do a thorough investigation of the exact dose measurements using optically stimulated dosimeters, thermoluminescent dosimeters, and simulation with Monte Carlo N-particle transport code to assess the skin and total body effective dose typical of portable XRF devices. We showed normal linear relationships between measurement time, x-ray tube current, and radiation dose with the device, and showed a second order polynomial relationship with increasing voltage and radiation dose. Dose was quantified using TLD, OSLD, and simulations, which gave similar dose estimations. Skin dose for a standard 50 kV 40 uA measurement for bone and toenail *in vivo* was 48.5 and 28.7 mSv according to simulation results. Total body effective dose was shown as 3.4 and 2.0 uSv for *in vivo* bone and toenail measurements for adults using the portable XRF device.

Introduction

Portable x-ray fluorescence (XRF) devices are being used more frequently for *in vivo* measurements to assess metal exposures in populations. The risks associated with the radiation exposure of these low energy x-ray tubes are minimal, but since they are used in population studies, a more thorough review of the radiation exposure would be appropriate to fully consider the radiation exposures associated with the use of portable x-ray fluorescence devices.

Metal exposure assessment has been performed for decades using x-ray fluorescence. Previous devices for x-ray fluorescence measurements used radioisotopes as a source to

[*]Corresponding author: Aaron Specht, 655 Huntington Ave Building 1 Rm 1402, Boston, MA 02115, aspecht@hsph.harvard.edu.

Conflicts of Interest:
The authors declare no conflicts of interest.

stimulate the characteristic x-ray emissions (Chettle, Scott, & Somervaille, 1991). Particularly the cadmium-109 radioisotope K-shell XRF device for lead measurement had well characterized radiation dose, which was summarized in a previous study (Huiling Nie, Chettle, Luo, & O'Meara, 2007). The radiation dose associated with portable XRF measurements has not been characterized as accurately and thoroughly. Only one previous study has explored the radiation dose of measurements using thermoluminescent dosimeters (H. Nie et al., 2011). However, it was quickly found after optimization of the device that the x-ray tube current used for this measurement was not optimal, and changes in x-ray tube settings were proposed for future studies and further changes are likely in the future to optimize for different metal or tissue measurements (Aaron James Specht, Weisskopf, & Nie, 2014).

Portable XRF presents a unique problem since the device uses a modifiable source, which can be used on different tissues to measure different biomarkers of exposure. Changes to the source or tissue examined would result in changes to the radiation dose and radiosensitive organs in the measurement. In this study, we measured radiation dose from a portable XRF, and identified the changes in dose with different x-ray tube voltage, current, and filtration when doing bone lead and toenail metal measurements.

2. Materials and Methods

2.1 Portable XRF Device

We used a Thermo Fisher XL3t GOLDD+ portable XRF device for this study (Thermo Fisher Inc., Billerica, MA). The device is typically used commercially for mining and soil measurements, but has been investigated for use in metal exposure assessment in vivo. This study focuses on *in vivo* uses and the associated radiation dose. This same x-ray system has been used in previous studies measuring bone *in vivo* for strontium and lead, and for measuring toenail *in vivo* for mercury and manganese (A. J. Specht et al., 2016; Aaron J. Specht, Mostafaei, Lin, Xu, & Nie, 2017; Aaron James Specht et al., 2014; Zhang, Specht, Weisskopf, Weuve, & Nie, 2017). For this study we used variable voltage, current, and filters from the device, which we note in the results for our measurements. The maximum power output of the x-ray tube was 2 watts.

2.2 Standard Phantoms

Soft tissue and bone equivalent phantoms were used in this study to determine the dose for *in vivo* bone measurements. Lucite plate phantoms were used to simulate soft tissue over bone by placing the Lucite under the flat surface of the bone phantoms in increments of 1 mm up to 5 mm of Lucite thickness. These Lucite plates were found to be an acceptable phantom for soft tissue in our previous study (Aaron James Specht et al., 2014). Cylindrical phantoms with a flat base for measurements were made of plaster of Paris were used to simulate bone. These measurements were made from the flat base of the phantom.

Toenail phantoms were made to test *in vivo* measurements of toenail metals. Standard phantoms for toenails were made using epoxy resin with added salt to standardize the attenuation coefficients, similar to prior work (Roy, Gherase, & Fleming, 2010; Zhang et al.,

2017). For the dose assessment we used toenail with 0.6 and 1.3 mm to determine the influence of toenail thickness on the radiation dose.

2.3 Optically Stimulated Luminescence Dosimetry System

For this study we used a Landauer InLight MicroStar Optically Stimulated Luminescence Dosimeter (OSLD) reader. This system has been used in studies of similar surface dose measurements in clinical practice (Yusof et al., 2015). The system was calibrated using standard OSLDs obtained from Landauer. Two calibrations were completed, one for low dose response (3 OSLDs between 10 and 1000 mRad), and one for high dose response (3 OSLDs between 1 and 1500 Rad). The measurements of calibration OSLDs were made 9 times to ensure accuracy, and it was found that there was < 2% change between readings, which fit the qualifications for clinical use of OSLD measurements according to TG-191 AAPM recommendations (AAPM, 2017). The OSLDs used for dose measurements were found to be accurate within 10% with repeated measures of the same x-ray settings measurement, which is primarily due to a higher background dose present in many of the OSLDs. Error from these measurements are represented in the figures as a measure of the error identified in our repeatability tests during measurements. We used these measurements to get a sense of the characteristic relationships between the portable XRF radiation dose and different situations, and did not expect a calibration of these OSLDs to produce quantified results within clinical level accuracy from this study.

We measured the radiation dose from a variety of settings and setups of phantoms. We first used a number of different geometries with the OSLDs in order to find the maximal dose. We measured the dose using x-ray tube settings 50 kV, 40 uA, and an iron and silver filter changing the time from 0.5, 1, 2, 3, and 4 minutes. We also did tests changing the current from 40 uA to 30, 20, 10 uA, while keeping the other settings the same. Then doing the other iterations changing the voltage to 40 kV and changing the current from 50 uA to 40, 30, 20, and 10 uA with filtration and time as constant. We did tests using aluminum and titanium, molybdenum and iron, and iron and silver filtration, which could prove to be useful for certain *in vivo* measurements.

Finally, we did dose measurements using 50 kV, 40 uA, and silver and iron filtration for bone and skin measurements. We used 0, 1, 3, and 5 mm of skin thickness to induce scatter. Then we used bare bone with no skin phantoms, 3mm skin with bone, and 5 mm skin with bone. We attempted to estimate surface bone dose by placing the OSLDs between the skin and bone phantom at 1, 2, 3, and 5 mm of skin. Lastly, we did tests of entrance and exit dose of toenail phantoms with thicknesses of 0.6 and 1.3 mm using both 50 kV 40 uA and 40 kV 50 uA x-ray tube setting with silver and iron filtration.

2.4 Thermoluminescent Dosimeters

Thermoluminescent dosimeters (TLDs) were used in this study for further validation of the dose readings. TLD 700 chips were used in this study, since the dose associated with XRF is purely from photons. The TLDs were read using a Harshaw TLD 4000 reader (Harshaw Partnership, Solon, OH, USA). The TLDs were calibrated against known exposures from a gamma irradiator at Purdue University. A Gammacell 220 (Nordian International Inc.)

containing a cobalt-60 radioisotope source with known exposure rates. Each TLD used in this study was separately irradiated for doses of 0, 25, 50, 75, 125, 250, 500, and 1000 mR, which were each measured 3 times to ensure the accuracy of the TLDs. The combined calibration curves of the TLDs produced a line with a correlation r^2 of 0.995, which gave us confidence in the quantification and accuracy of results obtained using these TLDs.

We first used a number of different geometries for measurement to find the maximal dose for the TLD measurements. The portable XRF comes standard with a camera, which can identify items placed in the field of view of the x-ray tube, which we used for verification of dosimeter placement consistency. We measured these dosimeters with x-ray tube settings of 50 kv, 40 uA, with an iron and silver filter for 3 minutes under soft tissue and bone phantoms, and 40 kv, 50 uA, with an iron and silver filter for 3 minutes under toenail, Lucite soft tissue phantoms, and bone phantoms. Finally, we used a grid pattern of 4 TLD chips to average over and better recreate our normalized skin area of 1 cm^2 (this approach approximated an area of ~0.8 cm^2).

2.5 Monte Carlo Simulations

We used the Monte Carlo simulation program, Monte Carlo N-Particle transport code (MCNP) in our study, which was developed by Los Alamos National Lab and distributed by the Radiation Safety Information Computational Center. This software has recently been updated to more accurately depict interactions at lower energies, using its default database for interaction cross-sections. This includes Doppler broadening effects and all interactions observed in XRF. In a previous study, we validated the use of this simulation to accurately simulate the output from the x-ray tube of the exact portable XRF used in this study (A. J. Specht, Weisskopf, & Nie, 2017). There was less than 9% difference between simulated and experimental spectral from that study. MCNP gives us the ability to set unique materials, densities, geometries, and sources in order to reproduce an experimental setup, and in the case of this study, to reproduce the dose of *in vivo* measurements. Previous studies have similarly used MCNP to estimate dose to patients in clinical settings (Yoriyaz, Stabin, & dos Santos, 2001). We used the same x-ray tube simulation as our previous study, but added in skin, bone, or toenail based on the specifications for our study. We did simulations to reproduce the *in vivo* bone measurements, and give estimates for bone and skin dose. We also did simulations of toenail *in vivo* measurements to look at skin dose below the toenail. The bone and skin composition and densities were taken from ICRU-44, and the toenail composition was taken from Rutherford and Hawk (Rutherford & Hawk, 1907).The simulation included a 40 cm long leg, which was used in full for energy deposition measurements in the total body effective dose calculations. For skin dose, only a $1cm^2$ voxel of the skin in the maximal area of exposure was used for dose measurements. In the calculations of dose, we used the number of particles that would have been used in the x-ray tube based on the amperage and a time of 3 minutes, which should make the measurements equal to those with TLDs and OSLDs with 3 minute exposures.

2.6 Total Body Effective Dose Calculations

We calculated total body effective dose for the bone measurement using the simulation to get total skin and total surface bone dose from the simulated 40 cm long leg. For the toenail

measurements, we assumed the same area of exposure except with the added attenuation of toenail. The dose from the bone was assumed to be all surface dose, since the penetration depth of x-rays from the portable XRF would only be ~0.5 mm into the bone. We used a simulation with skin (skin thickness 5 mm) and bone tissue 40 cm in length (bone radius 1.25 cm) to ensure we captured the full dose of any scattering that occurred. We approximated the total body bone surface using different values for 5-year-old, 10-year-old, and adult females and males. Five-year-old male and female bone area was taken from Specker *et al.* (Specker, Johannsen, Binkley, & Finn, 2001) to be 950 and 935 cm^2 respectively. For adult males and females we used a 2013 CDC report on Total Body Bone Area with values 1385 and 1399 cm^2 for 10 year olds and 2272 and 1918 cm^2 for adults (Looker et al., 2013). We assumed the density of bone was 1.7, 1.75, and 1.8 g cm^{-3} for 5-year-old, 10-year-old, and adult, respectively, as taken from the table on page 37 of ICRP 70 (ICRP, 1995). For skin areas we used 0.78, 1.12, and 1.90 m^2 for 5-year-old, 10-year-old, and adult, respectively ("Basic anatomical and physiological data for use in radiological protection: reference values. A report of age- and gender-related differences in the anatomical and physiological characteristics of reference individuals. ICRP Publication 89," 2002). We also included a comparison of total body effective dose with different tissue thickness values of 1, 3, and 5 mm.

3. Results

3.1 OSLD Results

Figure 1 below shows the linear dose relationship with measurement times using 50 kV, 40 uA, and iron and silver filtration. Figures 2, 3, and 4 show the significant non-linear relationship between dose and changes in voltage of the portable XRF device with constant 40 uA and iron and silver, molybdenum and iron, and aluminum and titanium filtration. Figure 5 shows the linear relationship between measured dose and current keeping 40 kV and the iron and silver filtration constant. Finally, Figure 6 shows the relationship between surface bone dose and skin thickness, which decreased slightly with increasing skin thickness. Increasing the skin thickness over the dosimeters, which would potentially increase scatter, did not increase the dose measured by the OSLD. The 1 cm^2 skin dose measurements using aluminum and titanium, molybdenum and iron, and iron and silver filtration at 50 kV 40uA and 3-minutes were 224.7, 49.0, and 103.7 mSv, respectively.

3.2 Thermoluminescent Dosimeter Measurements

We took measurements using TLDs to look at the radiation dose for *in vivo* measurements of toenail and bone with 2 separate measurements for each. The results for these measurements are summarized in Table 1 below. The average result from a grid of 4 TLD chips (~0.8 cm^2 area) arranged over the irradiated area during a bone and toenail measurement changed the dose to 48.8 and 43.3 mSv respectively. The differences in dose quantification are explained in the discussion.

3.3 Simulation Dose Measurements

We used the simulation to calculate the dose of the bone surface and skin, which would be the only components that would have radiation dose from *in vivo* measurements using the

portable XRF. Using this, we can then calculate total body effective dose for our measurements. The results for the measurements of skin dose and total body effective dose for bone and toenail measurements are shown in Table 2. The leg was 40 cm in length to capture all scatter, but for the skin dose only a 1 cm^2 voxel was used to determine skin dose. For total body effective dose, we used energy deposition in skin and bone surface, which we averaged over the previously mentioned total body skin and bone surface areas to arrive at the final values. We assume all the dose going to the bone is surface dose, surface bone and skin is the only contributing factors for total body effective dose in bone measurements, and the skin dose is the only contributing factor to total body effective dose from the toenail measurements. We conservatively used female average values for 5-year-old, male for 10-year-old, and female for adult calculations to report the highest possible dose. The simulation resulted in a bone dose averaged over the simulated leg (40 cm long and 1.25 cm radius) of 2.2, 2.2, and 2.1 mSv for 5-year-old, 10-year-old, and adult respectively. The simulated skin dose averaged over the total leg was 1.1 uSv. Changing the tissue thickness and bone surface dose resulted in a total body effective dose of 3.4, 3.7, and 4.3 uSv at 5, 3, and 1 mm tissue thickness respectively.

3.4 *In Vivo* Dose Measurement Comparisons

Table 3 shows a side-by-side comparison of the skin dose estimates made by measuring the dose with simulation, TLDs, and OSLD and their respective volume differences.

4. Discussion

This study determined radiation doses from using portable XRF devices for *in vivo* measurements in order to determine the suitability for such use. We found the total body effective dose delivered by the device in a 3-minute measurement to be reasonable and skin dose to be at a level higher and more concentrated than typical of diagnostic exams, but far from any deterministic radiation risk. We demonstrated the relationship of the radiation dose from the device with increasing time, amperage, and voltage in the x-ray tube, and the effect of different filtration on the radiation dose. Finally, we used simulations to determine and compare the experimental measures of skin and total body effective dose measurements.

One limitation of our experimental results from the study is accounting for slight geometry changes in the measurements. The x-ray tube aperture is quite small, and for this reason, it was potentially easy to place a TLD or OSLD in a spot that did not reflect the highest potential dose. To combat this issue, we initially did measurements with multiple TLDs and OSLDs to determine the geometry with the maximal dose. This maximal dose geometry is what we attempted to replicate for the other measurements as part of the study. However, it is hard to determine whether or not the maximal dose was captured for every measurement, but the simulation results would not have had this same issue.

Using our phantom measurements, we were able to identify dose distribution changes with skin thickness. As expected, bone dose would decrease with increasing skin thickness over bone, but the results show a linear relationship. Over the small thickness increases shown with *in vivo* measurements of about 5 mm, the exponential interaction with attenuation is approximately the same as a linear relationship. Using NIST values for the attenuation

coefficient of skin we can determine what the approximate dose changes should be with increases in skin thickness assuming a perfectly collimated beam, and at 5 mm of skin thickness the bone surface dose should be 65.9 mSv. We show a value of 31.4 mSv for the bone surface dose at 5 mm of skin thickness. This difference is likely due to the x-ray tube source collimation being imperfect, and the beam likely spreads over a larger area with increasing distance, similar to an inverse square effect.

There was an observable difference in dose quantification between TLD, OSLD, and simulation measurements. This is mainly attributable to the varying averaged volumes for the doses for each of these measurements, which is evidenced by our results using a grid of 4 TLD's, which gave results in line with are estimated volume changes. In the singular TLD and OSLD measurements, we are not averaging over a true 1 cm^2 area but are measuring about 0.2 cm^2. Since, the x-ray tube aperture of the portable XRF is actually smaller than 1 cm^2 it is likely most of the dose from entrance skin exposure of the x-rays will be more concentrated than this initial area limit. Another potential reason for the quantification differences is in the calibration procedure for TLD and OSLD measurements. The calibration was done on standard TLD or OSLD chips, which were under almost uniform exposure. Since the dose from the portable XRF is highly concentrated at one area of the dosimeter as mentioned above it could affect the reading of the TLD and OSLD. In addition, the OSLDs were calibrated from standard OSLDs obtained from the manufacturer, but ideally should be calibrated to include additional corrections due to fading, angular dependences, and beam-quality that could all play a role in the differences identified between the results. However, the main use of the OSLDs in our study was to study the relationships of the radiation dose with changes in the *in vivo* measurement, which should be consistent regardless of quantification issues.

The phantoms used as a proxy for skin, bone, and toenail in our experimental setup were not able to perfectly represent the radiation interactions of real skin, bone, or toenail. Lucite as a skin phantom was shown to be spectrally equivalent to cadaver skin in a previous study, but even considering this there are slight differences in attenuation and density. Similarly, the density and attenuation of plaster-of-Paris is not the same as bone, as discussed in an in-depth calibration study (Da Silva & Pejovic-Milic, 2017). The toenails were made to match attenuation coefficients of the characteristic x-rays of specific metals of interest between 5–11 keV, as discussed in previous studies, but the attenuation coefficients will vary as the energy changes from the energies of interest which will also change the scattering dose (Roy et al., 2010; Zhang et al., 2017). These differences will likely reflect an increase in the radiation dose from scatter of around 10 to 20% for the phantom measurements in comparison to true in vivo measurements due to the increased scatter cross sections for the phantoms. Considering the majority of the dose likely arises from direct interaction with the initial x-ray beam and the use of phantoms showed minimal increase in dose, we can accept these measurements and relationships to be slightly more conservative than true *in vivo* dose measurements. The simulation used accurately depicted human compositional and density data and included a life-size human leg for total body effective dose quantification, so simulation results should be the most accurate in terms of comparisons to radiation dose experienced in a true *in vivo* measurement.

Using the total body effective dose, we can estimate the risk of radiation-induced cancers. The increased risk for cancer and other inheritable effects from radiation has been found to be 5% per Sievert of total body effective dose (ICRP., 2007). Given the doses we found form the 3-minute portable XRF measurement, this would mean a 0.000004%, 0.000003%, and 0.000002% increased risk of cancer for 5-year olds, 10-year olds, and adults (ICRP., 2007).

Deterministic effects from skin dose have been shown to occur for doses in excess of 2 Gy according to ICRP publication 85, which the portable XRF skin dose is 400 times less than (ICRP., 2000). This 2 Gy limit for skin doses is typically assigned assuming a uniform dose to an area; however, studies in radiation therapy patients have shown that when doses are limited to small areas, stem cells migrate from surrounding unaffected skin to repopulate the areas affected by DNA damage.(von Essen, 1969; Withers, 1967) More recent studies have shown this to increase the resiliency of normal tissues by up to a factor of 4, which in the use of the portable XRF would further reduce the unlikely possibility of deterministic skin damage due to the small radiation beam used for measurements.(Narayanasamy et al., 2017)

Given the minimal skin dose and total body effective dose associated with these measurements, even measurement times as high as 10-minutes could be considered while maintaining a reasonable limit for exposure. The limit for total body effective dose to any member of the public set by NRC CFR 20.1301 is at 1 mSv per year, which is 100–300 times more than given in a single 3-minute measurement from our device.

The total body effective dose measurements shown in Table 2 were taken as the highest dose considering differences in sex. We only had sex specific data for total body bone area, and were not able to find sex specific data for skin area. The dose difference between males and females was minor with the greatest difference in the adult calculation of total body effective dose of 2.9 uSv for males and 3.4 uSv for females. Ten-year-old males had higher dose due to lower total bone area, since females typically have more growth earlier than males due to puberty. Almost all of the total body effective dose arose from the absorbed dose in the surface of the bone.

The surface bone dose decreases slightly in relation to the overlying tissue thickness, and detection accuracy for *in vivo* metal measurements decreases with increasing skin thickness. For *in vivo* measurement, typically there is a tradeoff between accuracy of the measurement and radiation dose (Aaron James Specht et al., 2014). As the surface bone dose decreases, so does the signal that arises from the bone, which in-turn increases the uncertainty of the metal quantification measurement. In our previous study, we found 3-minute measurements with 50 kV and 40 uA would achieve reasonable detection limits for populations with skin thickness lower than 5 mm (Aaron James Specht et al., 2014). In further application of the device, we found this to be a less reasonable assumption for all populations (A. J. Specht et al., 2016). With the results shown here, it seems that longer measurement times of up to 10 minutes would be feasible while maintaining acceptable radiation dose limits. This would reduce the detection limit by a factor of the square root of the increase in time or current, which in this case would be a decrease of a factor 1.8. However, we need to make sure the increased measurement times would not be overexposing those with low tissue thickness in order to capture a greater proportion of the population. Our results indicate that the dose

change for individuals with lower soft tissue thicknesses is relatively minor with an increase of about 0.8 uSv total body effective dose from 5 mm to 1 mm tissue thickness for a 3-minute measurement. The detection limit change over this tissue thickness difference is much more drastic with a detection limit of 11.0 and 1.8 ppm for 5 and 1 mm tissue thickness respectively (Aaron James Specht et al., 2014). This demonstrates that the primary limiting factors of the detection limit of the measurement come from a combination of the absolute efficiency of the detector, which decreases with the inverse square law from increasing tissue thickness, and the added attenuation from soft tissue thickness. The inverse square drop off with distance is a result of the characteristic x-ray production in the bone being isotropic, which will greatly decrease the efficiency of the detector with increasing distance from the characteristic x-rays arising in the bone. The added attenuation is a larger factor for the outgoing x-ray signal, since the initial x-ray beam is of higher average energy than the characteristic x-ray signal. Thus, the x-ray signal would have a higher interaction cross-section and probability of attenuation with increases in tissue thickness. Although our results indicate the radiation dose and total number of interactions creating signal in the bone will change, that relationship is almost linear over the range of tissue thicknesses in general population, and will have limited impact on increases in the detection limit in comparison to the changes induced by the inverse square effect and outgoing signal attenuation.

5. Conclusion

This study looked at the radiation dose administered while taking *in vivo* metal measurements with a standard 2-watt silver x-ray tube. We showed normal linear relationships between measurement time, x-ray tube current, and radiation dose with the device, and showed a second order polynomial relationship with increasing voltage and radiation dose. Dose was quantified using TLD, OSLD, and simulations, which gave similar dose estimations. Skin dose for a standard 50 kV 40 uA measurement for bone and toenail *in vivo* was 48.5 and 28.7 mSv according to simulation results. Total body effective dose was shown as 3.4 and 2.0 uSv for *in vivo* bone and toenail measurements for adults using the portable XRF device with a 3-minute measurement.

6. Acknowledgements

This work was supported by the National Institute of Environmental Health Science (NIEHS) R21 grant R21ES024700. The authors would like to thank the radiological and environmental management (REM) department at Purdue University and the Environmental Health and Safety (EH&S) health physics staff for the support and equipment in the study.

Sources of Funding:

This work was supported by the National Institute of Environmental Health Science (NIOSH) R21 grant R21ES024700.

7. References

American Association of Physicists in Medicine. Recommendations on the Clinical Use of Luminescent Dosimeters (TG191). Task Group No. 191 - AAPM AAPM Committee Tree: 2017.

Basic anatomical and physiological data for use in radiological protection: reference values. A report of age- and gender-related differences in the anatomical and physiological characteristics of

reference individuals. ICRP Publication 89. (2002). Ann ICRP, 32(3–4), 5–265. [PubMed: 14506981]

Chettle DR, Scott MC, Somervaille LJ. Lead in bone: sampling and quantitation using K X-rays excited by 109Cd. Environ Health Perspect 91: 49–55; 1991. [PubMed: 2040251]

Da Silva E Pejovic-Milic A Calibration of the (125)I-induced x-ray fluorescence spectrometry-based system of in vivo bone strontium determinations using hydroxyapatite as a phantom material: a simulation study. Physiol Meas, 38(6), 1077–1093; 2017 10.1088/1361-6579/aa63d3 [PubMed: 28248197]

International Commission on Radiation Protection. Basic anatomical and physiological data for use in radiological protection - the skeleton. Oxford: Pergamon Press; ICRP Publication 70, Annals of the ICRP, 25(2); 1995.

International Commission on Radiation Protection. Avoidance of Radiation Injury from Medical Interventional Procedures. Oxford Pergamon Press; ICRP Publication 85, Annals of the ICRP, 30(2); 2000.

International Commission on Radiation Protection. The 2007 Recommendations of the International Commission on Radiological Protection. Oxford: Pergamon Press; ICRP Publication 103, Annals of the ICRP, 37(2–4); 2007.

Looker AC, Borrud LG, Hughes JP, Fan B, Shepherd JA, Sherman M. Total body bone area, bone mineral content, and bone mineral density for individuals aged 8 years and over: United States, 1999–2006. Vital Health Stat 11(253), 1–78; 2013.

Narayanasamy G, Zhang X, Meigooni A, Paudel N, Morrill S, Maraboyina S,… Penagaricano J. Therapeutic benefits in grid irradiation on Tomotherapy for bulky, radiation-resistant tumors. Acta Oncol, 56(8), 1043–1047; 2017 10.1080/0284186X.2017.1299219 [PubMed: 28270018]

Nie H, Chettle D, Luo L, O'Meara J. Dosimetry study for a new *in vivo* X-ray fluorescence (XRF) bone lead measurement system. Vol. 263, pp. 225–230; 2007 Nuclear Instruments and Methods in Physics Research B

Nie H, Sanchez S, Newton K, Grodzins L, Cleveland RO, Weisskopf MG. In vivo quantification of lead in bone with a portable x-ray fluorescence system--methodology and feasibility. Phys Med Biol, 56(3), N39–51; 2011 10.1088/0031-9155/56/3/N01 [PubMed: 21242629]

Roy CW, Gherase MR, Fleming DE. Simultaneous assessment of arsenic and selenium in human nail phantoms using a portable x-ray tube and a detector. Phys Med Biol, 55(6), N151–159; 2010 10.1088/0031-9155/55/6/N02 [PubMed: 20182007]

Rutherford T, Hawk P. Comparative chemical composition of the hair of different races. J. Biol. Chem, 3, 459–489; 1907.

Specht AJ, Lin Y, Weisskopf M, Yan C, Hu H, Xu J, Nie LH. XRF-measured bone lead (Pb) as a biomarker for Pb exposure and toxicity among children diagnosed with Pb poisoning. Biomarkers, 21(4), 347–352; 2016 10.3109/1354750X.2016.1139183 [PubMed: 26856822]

Specht AJ, Mostafaei F, Lin Y, Xu J, Nie LH. Measurements of Strontium Levels in Human Bone In Vivo Using Portable X-ray Fluorescence (XRF). Applied Spectroscopy, 0003702817694383; 2017 10.1177/0003702817694383

Specht AJ, Weisskopf M, Nie LH. Portable XRF technology to quantify Pb in bone in vivo. Journal of Biomarkers, 2014, 9 pages; 2014.

Specht AJ, Weisskopf MG, Nie LH. Theoretical modeling of a portable x-ray tube based KXRF system to measure lead in bone. Physiol Meas, 38(3), 575–585; 2017 10.1088/1361-6579/aa5efe [PubMed: 28169835]

Specker B, Johannsen N, Binkley T, Finn K. Total body bone mineral content and tibial cotrical bone measures in preschool children. Journal of Bone and Mineral Research, 16(12); 2001.

von Essen CF. Radiation tolerance of the skin. Acta Radiol Ther Phys Biol, 8(4), 311–330; 1969. [PubMed: 5351216]

Withers HR. The dose-survival relationship for irradiation of epithelial cells of mouse skin. Br J Radiol, 40(471), 187–194; 1967 10.1259/0007-1285-40-471-187 [PubMed: 6019041]

Yoriyaz H, Stabin MG, dos Santos A. Monte Carlo MCNP-4B-based absorbed dose distribution estimates for patient-specific dosimetry. J Nucl Med, 42(4), 662–669; 2001. [PubMed: 11337557]

Yusof FH, Ung NM, Wong JH, Jong WL, Ath V, Phua VC., Ng KH. (2015). On the Use of Optically Stimulated Luminescent Dosimeter for Surface Dose Measurement during Radiotherapy. PLoS One, 10(6), e0128544; 2015. 10.1371/journal.pone.0128544 [PubMed: 26052690]

Zhang X, Specht AJ, Weisskopf MG, Weuve J, Nie LH. Quantification of manganese and mercury in toenail in vivo using portable X-ray fluorescence (XRF). Biomarkers, 1–7; 2017 10.1080/1354750X.2017.1380082

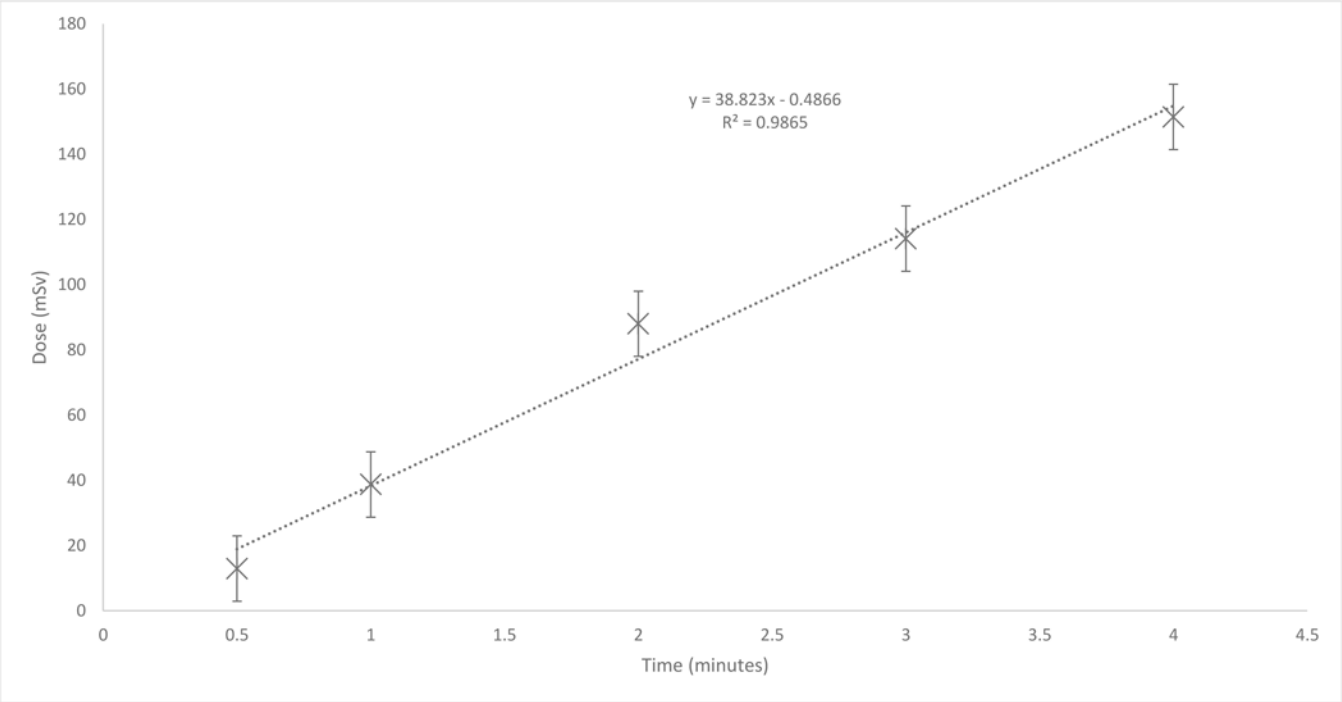

Figure 1.

Radiation entrance skin dose (0.2 cm^2) changes with different measurement times using 50 kV 40 uA and silver and iron filtration.

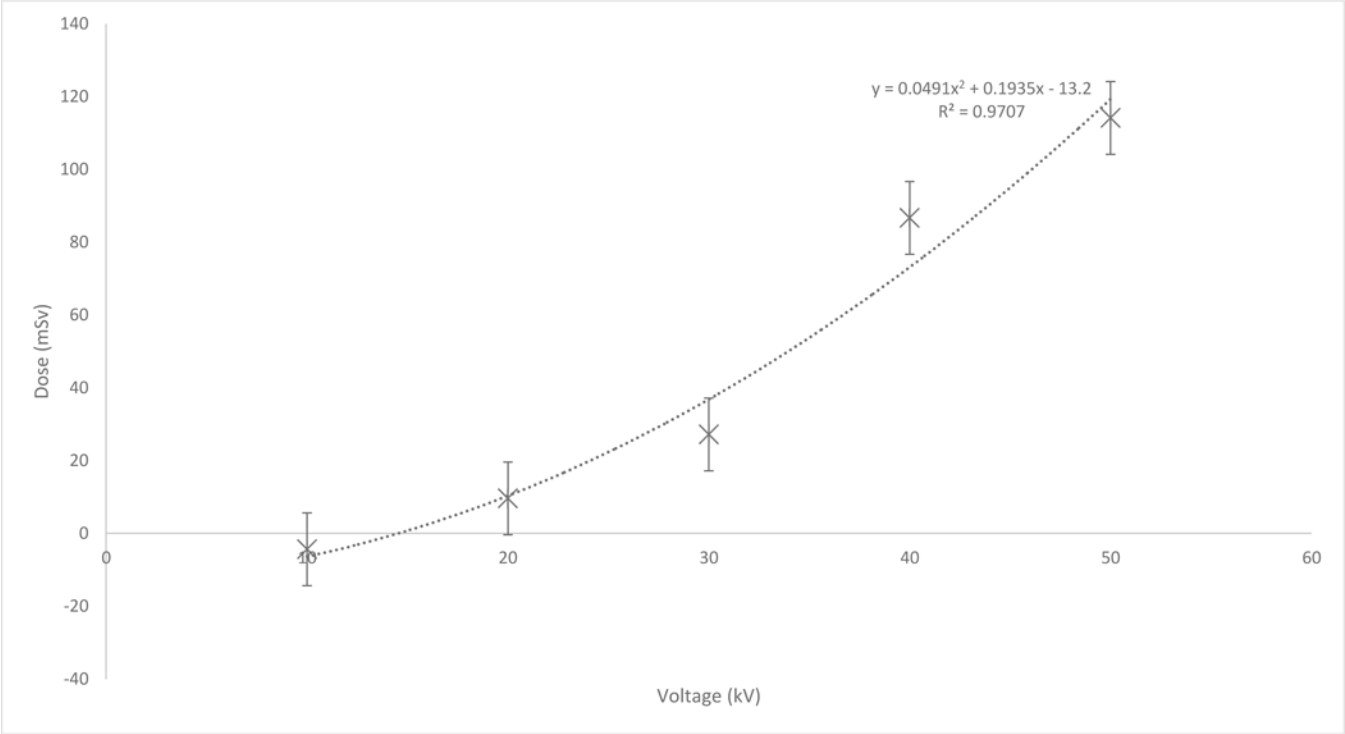

Figure 2.

Radiation entrance skin dose (0.2 cm^2) changes with different x-ray tube voltage settings using 40 uA and silver and iron filtration.

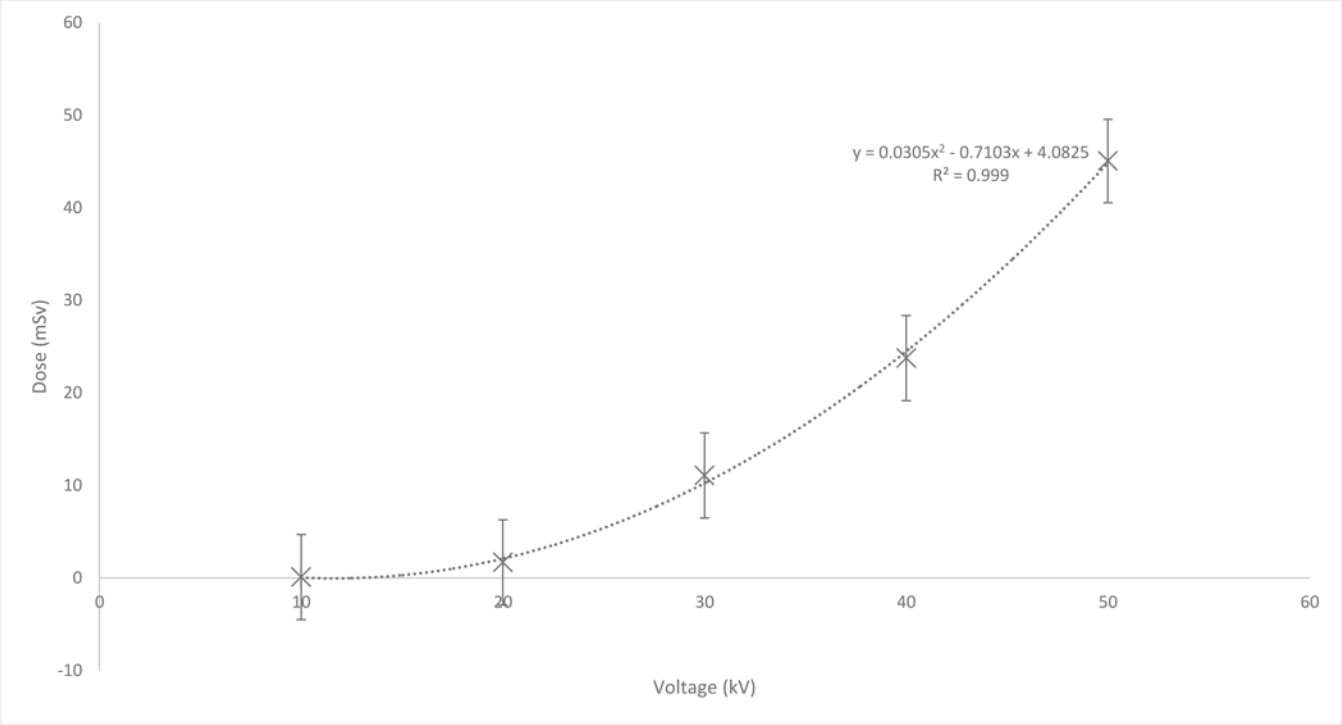

Figure 3.

Radiation entrance skin dose (0.2 cm^2) changes with different x-ray tube voltage settings using 40 uA and molybdenum and iron filtration.

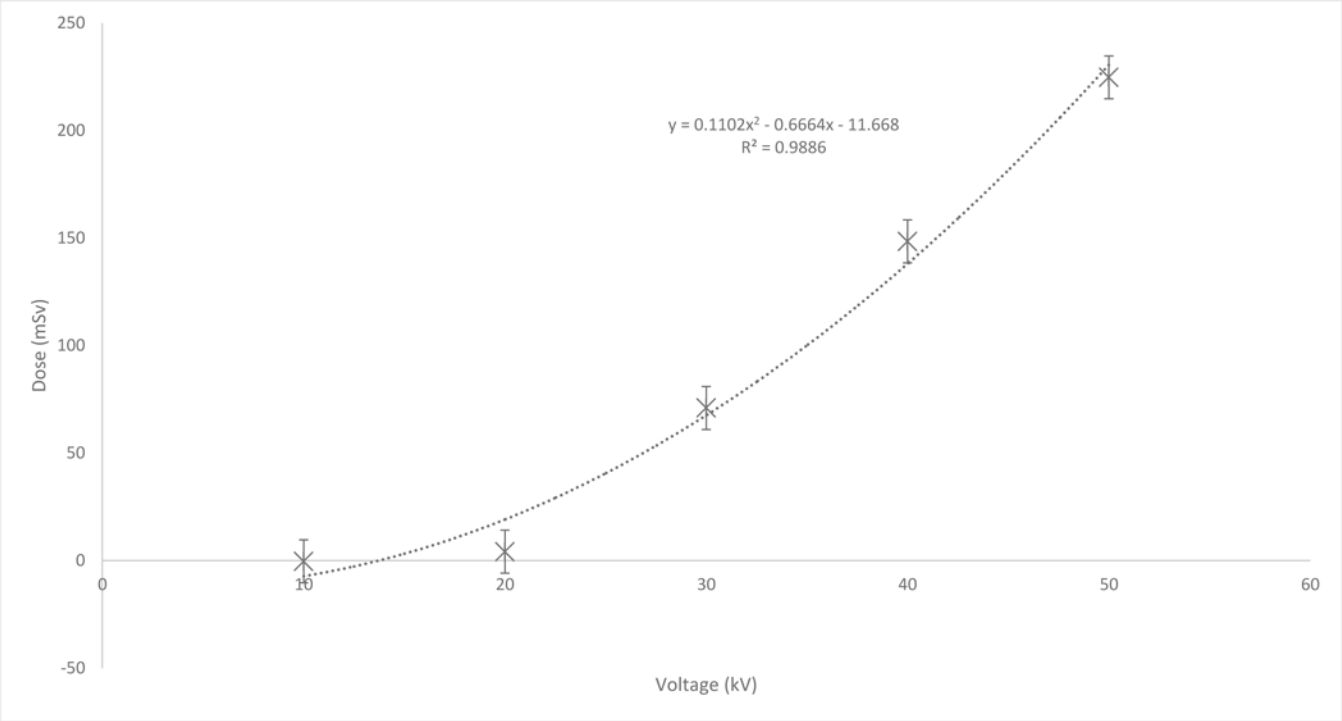

Figure 4.

Radiation entrance skin dose (0.2 cm^2) changes with different x-ray tube voltage settings using 40 uA and aluminum and titanium filtration.

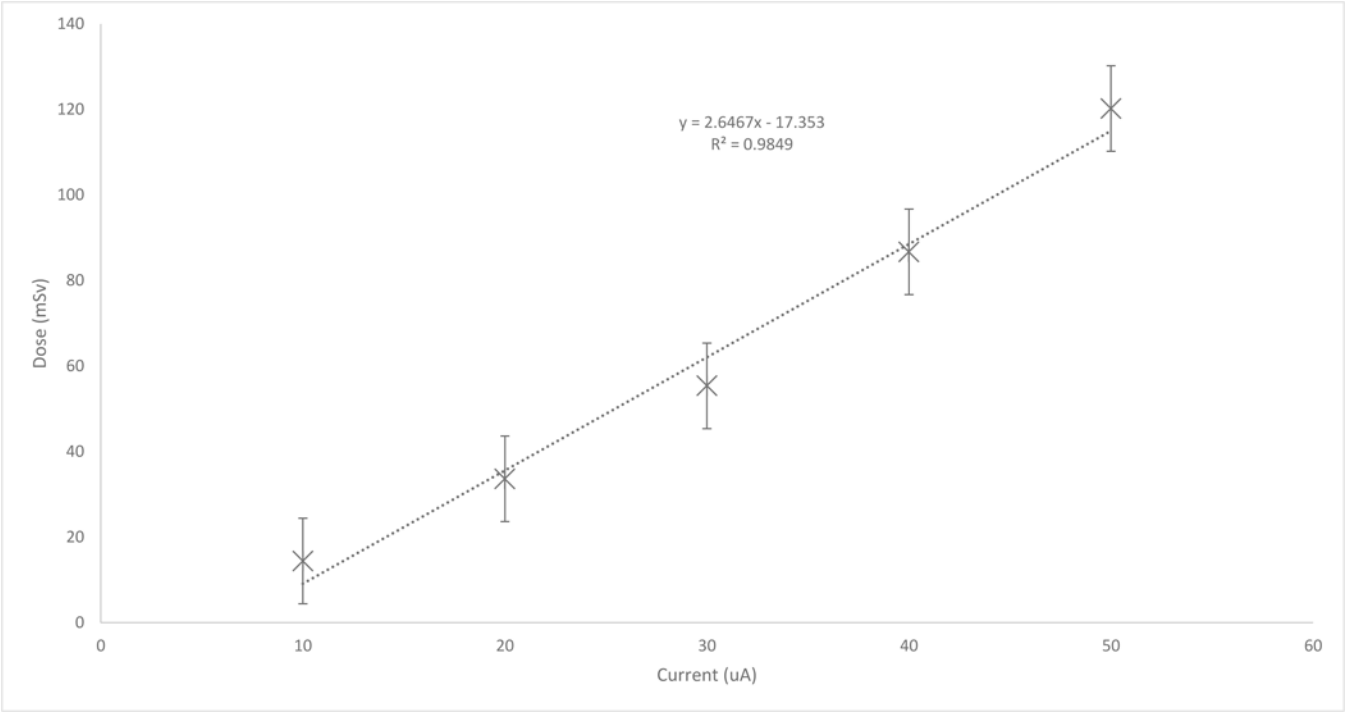

Figure 5.

Radiation entrance skin dose (0.2 cm^2) changes with different x-ray tube current settings using 40 kV and silver and iron filtration.

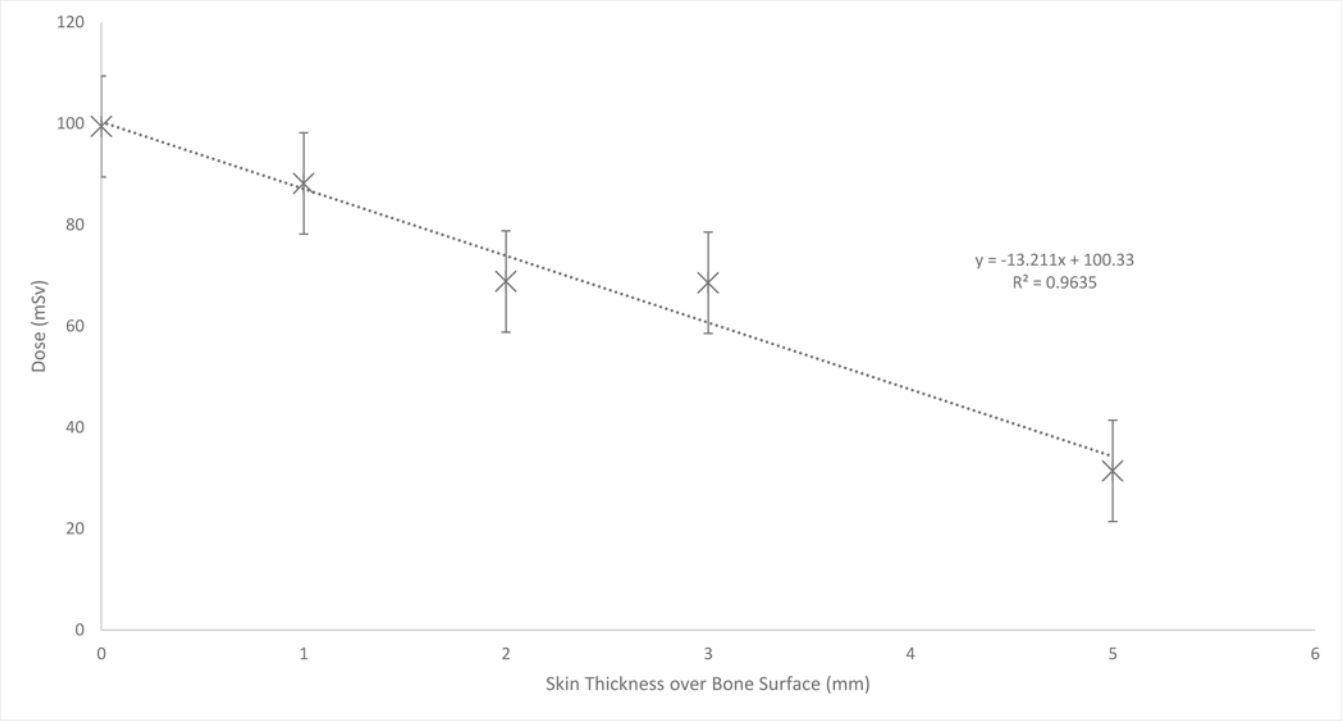

Figure 6.

Bone surface dose changes with increasing thickness of skin over bone using 50 kV, 40 uA, and silver and iron filtration.

Table 1.

Skin dose to 0.2 cm^2 with measurements of bone and toenail *in vivo* measurements.

	Dose Measurements (mSv)	
Measurement	**5mm Skin with Bone**	**1.3 mm Toenail**
1	73.9	67.9
2	60.2	61.7

Table 2.

Skin, bone, and total body effective dose for bone and toenail portable XRF measurements.

Total Body Effective Dose (uSv)		
	Bone Measurement	**Toenail Measurement**
5-year-old	7.4	4.4
10-year-old	4.9	2.9
Adult	3.4	2.0

Table 3.

Skin dose measurements for *in vivo* portable XRF measurements using different measurement techniques.

		Dose Estimates (mSv)		
	TLD (0.2 cm^2)	**TLD (~0.8 cm^2)**	**OSLD (0.2 cm^2)**	**Simulation (1 cm^2)**
Bone Measurement	73.9	48.8	103.7	48.5
Toenail Measurement	67.9	43.3	111.7	28.7